EPJ Web of Conferences **67**, 02111 (2014)
DOI: 10.1051/epjconf/20146702111

On transonic flow models for optimized design and experiment

Jiří Stodůlka[1,a], Helmut Sobieczky[2]

[1]CTU in Prague, FME, Department of Fluid Dynamics and Thermodynamics, Prague, Czech Republic
[2]TU Vienna, Institute of Technology, Vienna, Austria

Abstract. In the paper the near sonic flow theory for flows with small perturbations to sonic parallel flow is developed. This theory stands on the basis of potential flow of a compressible fluid and enables to receive an exact solution of the flow parameters past transonic cusped airfoils and their geometrical description. Generated airfoil shapes are tested using CFD ANSYS Fluent code to validate the results. Obtained numerical results from all-round commercial code show good accordance with the theory and confirm their value for future work in transonic design.

1 Introduction

Among various aerospace vehicle speeds, the transonic regime has always posed remarkably difficult challenges to systematic design and experimental techniques. Theoretical methods to understand transonic flow phenomena developed in past time shed light into transonic testing techniques, by solving the underlying physical relations, in various stages of their simplifications. Such analytical models led to the geometrical description of basic airfoil shapes and subsequently to realistic wing sections including qualitative insight into the structure of surrounding transonic flow. At the same time, numerical simulations of these physical relations were developed so that prior to experimental investigations quantitative results were obtained. These, finally, allow for a calibration of windtunnels which are needed to aid the industry in their development of efficient flight vehicles. In this contribution we try to remember some analytically defined methods and airfoil geometries as test cases and compare analytical flow description with numerics, making use of a commercially available computational fluid dynamics code. Our final goal is to arrive at a high degree of understanding typical transonic challenges so that accelerated optimization strategies may be carried out with a reduced set of input parameters, before costly experiments may focus on optimum design cases.

2 Near Sonic Flow Theory

This chapter was written using [1]. The steady state two-dimensional potential flow is defined by the continuity equation and irrotationality.

$$div\,(\rho,\vec{v}) = 0 \tag{1}$$

$$rot\,(\vec{v}) = 0\,. \tag{2}$$

We define velocity potential ϕ and stream function ψ with $q = |\vec{v}|$ and ϑ the flow angle.

$$\phi_x = \frac{\rho_0}{\rho}\psi_y = u = q\cos\vartheta \tag{3}$$

$$\phi_y = -\frac{\rho_0}{\rho}\psi_x = v = q\sin\vartheta \tag{4}$$

where density as function of Mach number is [2]:

$$\frac{\rho}{\rho_0} = \left(1+\frac{\gamma-1}{2}M^2\right)^{-\frac{1}{\gamma-1}}. \tag{5}$$

This system (3) and (4) of nonlinear Cauchy-Riemann equations or so-called Beltrami equations after elimination of ψ and ϕ yields:

$$\phi_{xx}+\phi_{yy} = -\frac{\rho_x}{\rho}\phi_x - \frac{\rho_y}{\rho}\phi_y \tag{6}$$

$$\psi_{xx}+\psi_{yy} = \frac{\rho_x}{\rho}\psi_x + \frac{\rho_y}{\rho}\psi_y\,. \tag{7}$$

To avoid the nonlinearity of this basic system we transform the solution to the hodograph plane replacing the physical coordinates x, y with new ones, the flow angle ϑ and Prantl-Mayer turning angle υ with a* being the critical velocity.

[a] Corresponding author: jiri.stodulka@fs.cvut.cz

$$\upsilon = \int_{a^*}^{q} \sqrt{\left| M^2 - 1 \right|} \frac{dq}{q} . \tag{8}$$

These new variables lead to define a hodograph plane wherein the basic Beltrami system becomes linear:

$$\phi_\upsilon = K(\upsilon)\psi_\upsilon \quad (\upsilon \geq 0, M \geq 1), \tag{9}$$

$$\phi_\upsilon = -K(\upsilon)\psi_\upsilon \quad (\upsilon \leq 0, M \leq 1), \tag{10}$$

with

$$K = K\left(M(\upsilon)\right) = \frac{\rho_0}{\rho}\sqrt{\left| M^2 - 1 \right|} . \tag{11}$$

ϑ and υ are also functions of a computational working plane obtained from the basic υ, ϑ hodograph by conformal (subsonic) or characteristic (supersonic) mapping. For subsonic including sonic conditions conformal mapping defines working plane ζ. E is the mapping function.

$$\zeta_0 = \upsilon + i\vartheta, \tag{12}$$

$$\zeta = s + it = E(\zeta_0) . \tag{13}$$

The basic system in ζ becomes then:

$$\phi_s = -K(\upsilon(s,t))\psi_t \tag{14}$$

$$\phi_t = K(\upsilon(s,t))\psi_s . \tag{15}$$

$\upsilon(s,t)$ is then the real and $\vartheta(s,t)$ imaginary part of $E^{-1}(\zeta)$. These equations (14) and (15) form the linear Beltrami system and elimination of ψ and ϕ leads to a linear Poisson equations:

$$\phi_{ss} + \phi_{tt} = \frac{K_s}{K}\phi_s + \frac{K_t}{K}\phi_t , \tag{16}$$

$$\psi_{ss} + \psi_{tt} = \frac{K_s}{K}\psi_s + \frac{K_t}{K}\psi_t . \tag{17}$$

In the supersonic region new characteristic variables occur with a suitable mapping function H.

$$\xi = H(\vartheta + \upsilon) , \tag{18}$$

$$\eta = H(\vartheta - \upsilon) . \tag{19}$$

The system is then valid in ζ, η plane

$$\phi_\xi = K(\upsilon(\xi,\eta))\psi_\xi \tag{20}$$

$$\phi_\eta = -K(\upsilon(\xi,\eta))\psi_\eta \tag{21}$$

or

$$\left(\frac{d\psi}{d\phi}\right)_{\xi,\eta=const} = \pm K^{-1} . \tag{22}$$

That is the basic relation to integrate the flow equations for method of characteristics for supersonic flow. This solution allows the integration of physical coordinates x, y by

$$dz = dx + idy = e^{i\vartheta}\left(d\phi + i\frac{\rho_0}{\rho}d\psi\right)q^{-1} \tag{23}$$

for flows with small perturbations to a sonic parallel flow so that

$$(M-1) << 1 \tag{24}$$

$$\vartheta << \pi/2 \tag{25}$$

and by eliminating ψ and ϕ we can obtain a system for physical plane coordinates. The transonic similarity laws containing a similarity parameter σ for reduction of variables for place and state x, y, q, ϑ are:

$$S = \pm 2\cdot 3^{-1}\cdot\sigma^{-1}(\gamma-1)^{1/2} a\left|1 - \frac{q}{a^*}\right|^{3/2} , \tag{26}$$

$$T = \sigma^{-1}\cdot\vartheta , \tag{27}$$

$$X = \phi / a^* , \tag{28}$$

$$Y = \sigma^{-1/3}\cdot 3^{1/3}\left[2^{-1}(\gamma-1)\right]^{\frac{1}{\gamma-1}+\frac{1}{3}}\cdot\psi / a^* . \tag{29}$$

S is positive for supersonic, negative for subsonic and equal to zero for sonic conditions. The basic system (3) and (4) then yields to corresponding Beltrami system for reduced physical plane parameters S and T.

$$X_S = \pm\left| S^{1/3} \right| Y_T \tag{30}$$

$$X_T = \pm\left| S^{1/3} \right| Y_S \tag{31}$$

3 Exact Solution

Solving previous hodograph relations allows to derive the formulae defining the shape, flow conditions and pressure coefficient for cusped airfoils in a uniform sonic flow $M_\infty = 1$ [3]. The schematic wiev on a cusp with all defined parameters is on figure 3.1.

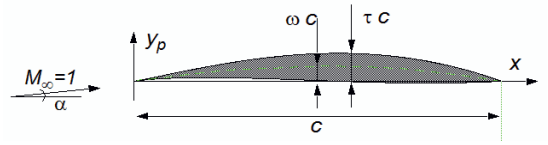

Figure 3.1. The cusp parameters.

Thickness to chord ratio is τ and chamber to chord ratio ω. The solution is exact for $\tau \to 0$ and practically valid for slender airfoils with $\tau \leq 0.5$. The case with chamber to chord ratio $\omega = 0$ is the symmetrical one also known as "Guderley's cusp". Limit of validity for chambered airfoils is given by ratio $\omega/\tau \leq 0.5$.

The chamber/thickness parameter is given by:

$$P\left(\frac{\omega}{\tau}\right)=2^{13/2}\cdot 3^{3/2}\cdot 5^{-7/2}\cdot\frac{\omega}{\tau}\left[1+2^{12}\cdot 3\cdot 5^{-6}\left(\frac{\omega}{\tau}\right)^{2}\right]^{-1/2} \tag{32}$$

When the cusp is chambered, it is pointing into the flow and it is smoothly passed by the stream so the flow is not forced to change direction around sharp leading edge. The angle of attack is then:

$$\alpha=\tau\cdot 2^{-9/2}\cdot 3^{-1/2}\cdot 5^{5/2}\cdot P\frac{1-2^{-1}\cdot 3^{-4}\cdot 5\cdot 13P^{2}}{(1-2^{-1}\cdot 3^{-2}\cdot 5P^{2})^{3/2}}. \tag{33}$$

The geometry vertex data for family of cambered airfoils is given by:

$$y_p(X)=\tau\cdot X(1-X)\left(2^{2}\cdot\frac{\omega}{\tau}\pm 2^{-2}\cdot 3^{-3/2}\cdot 5^{5/2}\cdot X^{1/2}\right). \tag{34}$$

and finally the pressure coefficient:

$$c_p=\frac{(5^{2}\cdot\tau)^{2/3}}{\left[2^{2}\cdot 3\cdot(\gamma+1)\right]^{1/3}}\cdot \left[\frac{(1-2^{-2}\cdot 3^{-2}\cdot 5P^{2})}{(1-2^{-1}\cdot 3^{-2}\cdot 5P^{2})}-2^{-1}\cdot 5X\mp\frac{2^{-1/2}\cdot 3^{-1}\cdot 5P\cdot X^{1/2}}{(1-2^{-1}\cdot 3^{-2}\cdot 5P^{2})^{1/2}}\right] \tag{35}$$

where γ is specific heat ratio.

4 Numerical Solution

For the numerical simulations the upcoming three variants of cusped airfoils were investigated. The symmetrical "Guderley's cusp", the limit variant with thickness to chord ratio τ = 0.1 and parameter ω/τ = 0.5 and last case with parameters somewhere in the middle of the exact solution bounds, τ = 0.05 and ω/τ = 0.02.

The computational domain was 20x the chord length in all directions. The mesh for all cases was mapped with quad cells with total count of approx. 100000 elements, except for the symmetrical case where only the half of the plane could be used. The detail of the mesh for one of the cases is shown on figure 4.1.

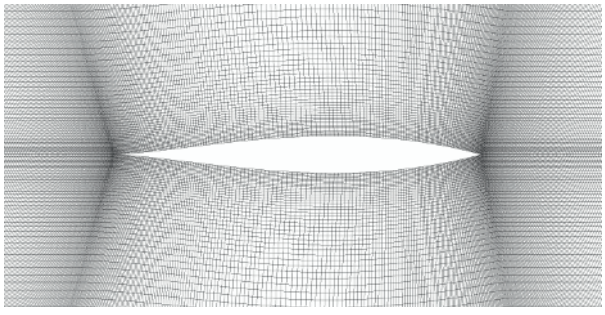

Figure 4.1. Quad computational mesh.

For flow simulations was used the inviscid – Euler model with ideal gas implemented in a commercial CFD software ANSYS Fluent. The numerical scheme was the AUSM. The only outer boundary condition was set as the pressure far field and it is computed using the gas dynamics equation [4]:

$$\frac{p_0}{p}=\left(1+\frac{\gamma-1}{2}Ma^{2}\right)^{\frac{\gamma}{\gamma-1}}. \tag{36}$$

Where p_0 is the total or atmospheric pressure and Mach number exactly one for this case. Pressure p then gives the value for the far field.

5 Results

All three tested cases successfully led to a converged solution using explicit solver after 10 – 15 thousand iterations. Contours of Mach number to visualise the simulated flow field are shown on figure 5.1. – 5.3. The most important thing that can be noticed from these figures is the fact that no shock appears anywhere near the leading edge or along the airfoils. The velocities at the leading edge are subsonic and along the airfoil the velocity continually rise to supersonic values what forms the obligue shocks propagating from the trailing edge. The flow is smooth for all cases along whole length as the theory suggests.

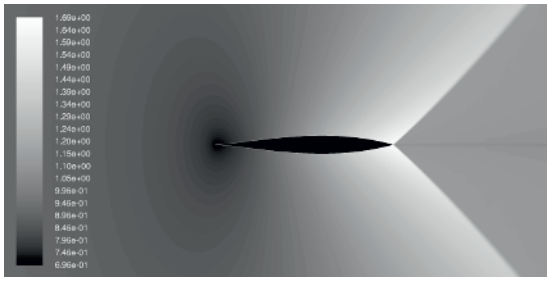

Figure 5.1. Contours of Mach number – symmetrical airfoil.

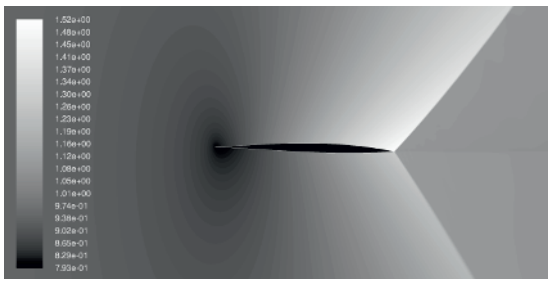

Figure 5.2. Contours of Mach number τ = 0.05, ω/τ = 0.02.

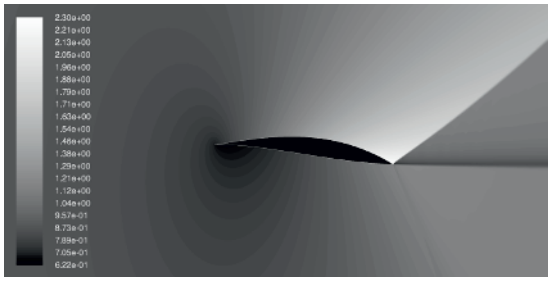

Figure 5.3. Contours of Mach number τ = 0.1, ω/τ = 0.5.

The differences between the cases are obvious and depend on the input thickness and chamber to chord ratio parameters. The flow for the symmetrical case is as expected symmetrical with two obligue shocks starting at the trailing edge, but for the thickest and most chambered limit airfoil the shock is formed only on the upper side of the airfoil while the flow is not accelerated enough along lower side and it remains shockfree till the end as the velocity near the end of the airfoil is similar to the velocity behind. The thin and less chambered case is somewhere between two previous variants as it forms two shocks but with different strength. With the rising thickness and chamber a higher Mach numbers are also reached.

The way how to compare the results with the theoretical ones is via the pressure coefficient c_p as described above. Theoretically correct pressure coefficient distribution on the airfoil surface is given by eq. (35) and figures 5.4. – 5.6 show the comparison with the numerical data. Dashed lines represent the theory and solid lines are results from the numerical simulation.

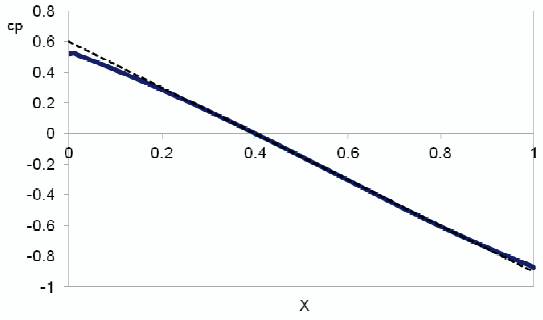

Figure 5.4. Pressure coefficient – symmetrical airfoil.

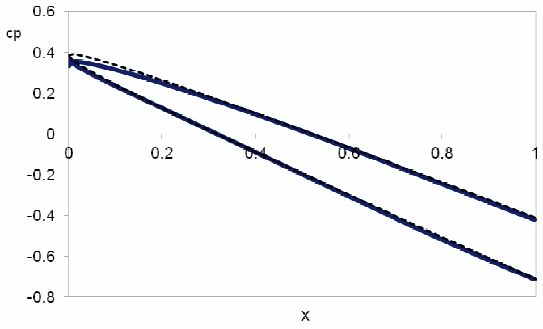

Figure 5.5. Pressure coefficient $\tau = 0.05$, $\omega/\tau = 0.02$.

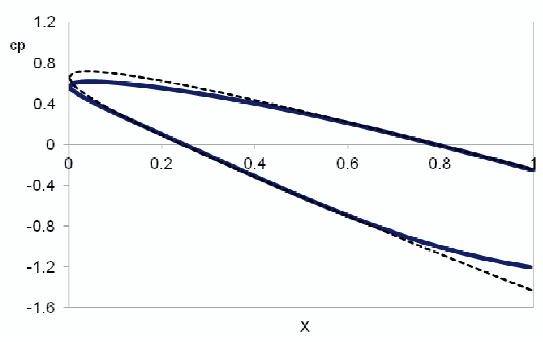

Figure 5.6. Pressure coefficient $\tau = 0.1$, $\omega/\tau = 0.5$.

From correct flow behavior already obvious from contour figures is expectable that the pressure coefficient distribution along the airfoil surface will also correspond at least tendentiously with the theoretical lines and data on figures 5.4. – 5.6. confirm that. In areas where pressure coefficient values lay between 0.3 and -0.8 are numerical results almost identical with dashed theoretical. As the values rise from these bounds noticeable deviations appear. Even when there is no flow separation on the leading edge and shocks appear only at the trailing edges so the character of the flow corresponds with the theoretical assumptions some differences appear right in these areas. This may be given by the fact that the flow speeds start to differ from a near sonic flow here as Mach numbers reached in these areas vary from 0.6 to 2.3. Inviscid Fluent code also probably allows the flow to be rotational, what the analytical potential flow neglect.

6 Conclusions

Theory of two-dimensional transonic flow past cusped airfoils was developed on the basis of compressible potential flow and it is used for optimized profile shape generation. The numerical experiment enables to receive data on parameters and flow structures past these airfoils. Obtained results confirmed well the accordance between numerical and exact analytical data by means of near sonic flow theory. More than any concrete practical value this work is aimed to show the possibility of using the already developed theories for creating first systematic designs that can be initial cases for optimized shapes for real prototypes. These cases in transonic regime are easily comparable with results obtained from modern CFD codes. These can be considered as useful, fast and reliable tool for future steps in transonic airfoils design and optimization.

References

1. M. Trenker, H. Sobieczky, Proc. Int. Symp on Inverse Problems in Engineering mechanics, Nagano (2001)
2. A. H. Shapiro, *The Dynamics and Thermodynamics of Compressible Fluid Flow*, The Ronald Press Company, New York (1957)
3. H. Sobieczky, ZAMP **26** (1975)
4. ANSYS Fluent 14.0 Users Guide, ANSYS, Inc., (2011)

Acknowledgement

This work has been supported by the Grant Agency of the Czech Technical University in Prague, grant no. SGS13/180/OHK2/3T/12